Geological Magazine

www.cambridge.org/geo

Original Article

Cite this article: Raeisi D, Mirnejad H and Sheibi M (2019) Emplacement mechanism of the Tafresh granitoids, central part of the Urumieh–Dokhtar Magmatic Arc, Iran: evidence from magnetic fabrics. *Geological Magazine* **156**: 1510–1526. https://doi.org/10.1017/S0016756818000766

Received: 30 January 2018
Revised: 24 September 2018
Accepted: 17 October 2018
First published online: 9 January 2019

Keywords:
I-type granitoids; emplacement; anisotropy of magnetic susceptibility; Indes and Talkhab faults; Urumieh–Dokhtar Magmatic Arc

Author for correspondence:
Hassan Mirnejad Email: hmirnejad@ut.ac.ir

CAMBRIDGE UNIVERSITY PRESS

Emplacement mechanism of the Tafresh granitoids, central part of the Urumieh–Dokhtar Magmatic Arc, Iran: evidence from magnetic fabrics

Davoud Raeisi[1], Hassan Mirnejad [1,2] and Maryam Sheibi[3]

[1]School of Geology, College of Science, University of Tehran, Tehran, Iran; [2]Department of Geology and Environmental Earth Sciences, Miami University, Oxford, Ohio, USA and [3]Faculty of Earth Sciences, Shahrood University of Technology, Shahrood, Iran

Abstract

Granitoid stocks crop out in the Ghahan and Sarbadan areas near Tafresh city, which is situated in the central part of the Urumieh–Dokhtar Magmatic Arc, Iran. The stocks, consisting of porphyritic and sub-granular diorite and granular granodiorite, intruded into Eocene volcano-sedimentary units. Normalized multi-element diagrams indicate that the analysed rocks are enriched in large-ion lithophile elements and depleted in high field strength elements. These geochemical features are typical of subduction-related calc-alkaline arc magmas. The stocks belong to the ferromagnetic and I-type granitoid series. Anisotropy of magnetic susceptibility provides information about the internal fabric of the granitoids. Susceptibility values range from 5.6×10^{-3} to more than 71.6×10^{-3}, averaging 27.9×10^{-3} SI. Relatively low anisotropy values (P%) rarely exceed 10 %. Shape parameters (T) vary between −0.48 and +0.74, averaging + 0.2. Each stock is interpreted to contain a distinct feeder zone in which magnetic lineation plunges steeply (> 60°), suggesting that the magma ascended mainly in a NW–SE conduit and, to a lesser extent, in an E–W direction. Integration of magnetic fabric data, field observations and tectonic setting indicates that the shear zone that was developed between the Indes and Talkhab faults had created an opening into which the Ghahan and Sarbadan stocks were emplaced by way of creating a suitable tensional space for the ascent of magma.

1. Introduction

The Urumieh–Dokhtar Magmatic Arc (UDMA), as a part of the Alpine–Himalayan orogenic belt, strikes NW–SE and lies parallel to the main Zagros Folded Thrust Belt in Iran (Fig. 1a). This magmatic arc, developed during subduction of the Neo-Tethys oceanic crust beneath the Iranian plate (Ricou *et al.* 1977; Dercourt *et al.* 1986; Alavi, 1994, 2004; Agard *et al.* 2011), has been active from Late Jurassic time up to the present (Berberian & King, 1981; Berberian *et al.* 1982). It comprises distinct linear, voluminous magmatic complexes along the formerly active margin of the Iranian plate (Stöcklin, 1968; Berberian *et al.* 1982; Alavi, 2007; Rezaei-Kahkhaei *et al.* 2011; Shafaii Moghadam & Stern, 2011). The UDMA contains a large number of batholiths, discrete plutons and sub-volcanic rocks of calc-alkaline affinity, similar to those of Andean-type magmatism (Förster *et al.* 1972; Berberian et al. 1982; Alavi, 2004). Although the relationship to subduction is clear (e.g. Berberian & King, 1981; Agard et al. 2005), the tectono-magmatic processes of magma emplacement in the UDMA have not been investigated to date. In general, understanding granite emplacement and deformation is challenging, because not all granitic rocks develop mesoscopic-scale deformation fabrics (Yakeu Sandjo *et al.* 2016). Of importance is the ‘space problem’, which may be resolved in situations where motion on faults and shear zones creates space for magma emplacement (see reviews by Hutton, 1988; De Saint-Blanquat *et al.* 2001). In the instance of the Tafresh granitoids, similar to the well-studied Papoose Flat pluton (De Saint-Blanquat *et al.* 2006), there is no evidence for this kind of structural control. In the latter case, the anisotropy of magnetic susceptibility (AMS) technique offers a suitable means to clarify the space problem. Indeed, numerous AMS studies of mafic and felsic rocks, both intrusive and extrusive, have demonstrated that this technique efficiently describes flow, strain fabrics and emplacement mechanisms (e.g. Tarling & Hrouda, 1993; Bouchez, 2000), and it is especially effective for igneous rocks whose foliation and lineation are difficult to observe and measure (e.g. the Tafresh granitoids), where no clear signs of deformation are present at the mesoscopic and field scales (Ellwood *et al.* 1980; Guillet *et al.* 1983; Bouchez *et al.* 1990; Tarling & Hrouda, 1993; Cruden & Launeau, 1994; Aranguren, 1997; Bouchez, 1997; Cruden *et al.* 1999; Yakeu Sandjo *et al.* 2016). Through magnetic techniques, precise and reproducible measurements of foliation and lineation can be applied to any outcrop in a pluton (Bouchez, 1997), from which magmatic flow directions

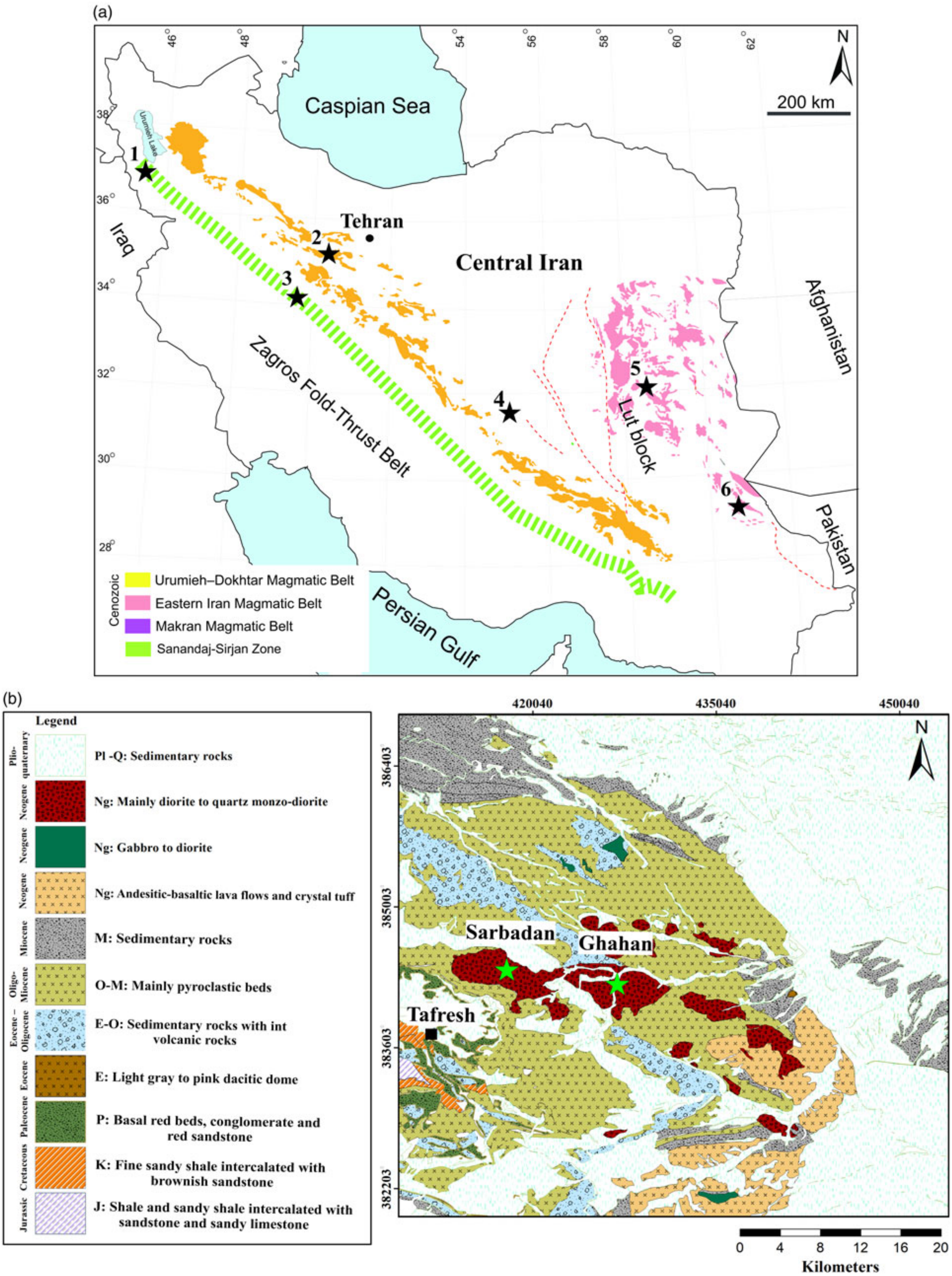

Fig. 1. (Colour online) (a) Simplified geological map of Iran (Aghanabati, 2004) and (b) geological map of the Tafresh area (modified after Hajian, 1977). The star shows the position of the plutons in Iran on which AMS was carried out. 1 – Urumieh (Ghalamghash *et al.* 2009); 2 – Tafresh (this study); 3 – Boroujerd and Gousheh (Rasouli *et al.* 2012); 4 – Shir-Kuh (Sheibi *et al.* 2012); 5 – Shah-Kuh (Esmaeily *et al.* 2007); 6 – Zahedan (Sadeghian *et al.* 2005).

https://doi.org/10.1017/S0016756818000766 Published online by Cambridge University Press

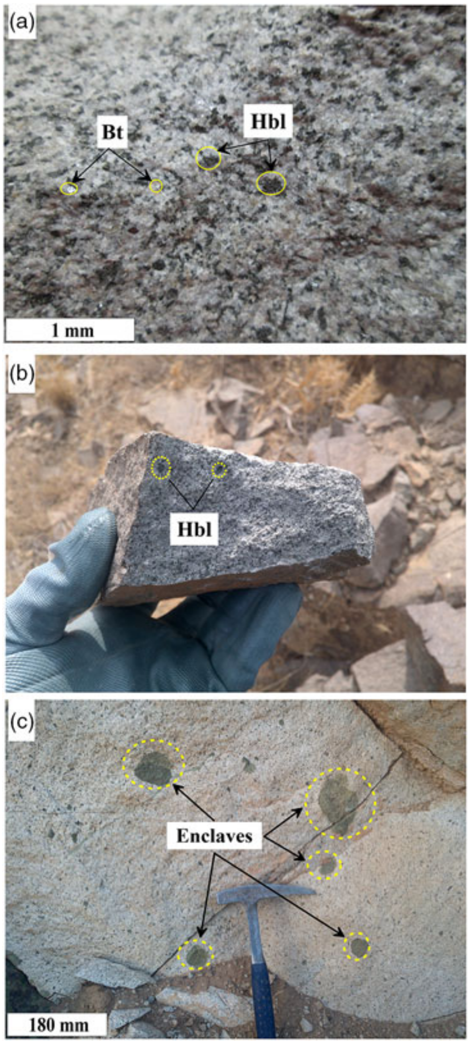

Fig. 2. (Colour online) Field relationships in the Tafresh granitoids. (a) Granodiorite with granular texture, Sarbadan stock. Hornblende (Hbl) and biotite (Bt) crystals are set in a matrix mainly composed of feldspar crystals. (b) Hand specimen of diorite, Ghahan. Hornblende (Hbl) in a matrix mainly composed of plagioclase crystals. (c) Fine-grained microdiorite enclaves in the diorite rock. Mineral abbreviations after Whitney & Evans (2010).

can be reconstructed via the orientation of the magnetic ellipsoids (e.g. Ellwood, 1978; Cañón-Tapia *et al.* 1996, 1997; Dragoni *et al.* 1997; Rochette *et al.* 1999).

In Iran, magnetic fabric studies by AMS have been in progress for more than 15 years. The first study focused on the emplacement mechanisms of the Zahedan pluton (Sadeghian *et al.* 2005), followed by studies of other plutons by other researchers (Shah-Kuh pluton, Esmaeily *et al.* 2007; Urumieh pluton, Ghalamghash *et al.* 2009; Shir-Kuh pluton, Sheibi *et al.* 2012; Boroujerd pluton, Rasouli *et al.* 2012; Gol-e-Zard pluton, Sadeghian *et al.* 2014; Challu pluton, Sheibi & Majidi, 2015; Panj-Kuh pluton, Sheibi & Pooralizadeh Moghadam, 2015). Most of these studies are in the Sanandaj–Sirjan Zone (SSZ), central Iran and SE Iran (Fig. 1). This paper is the first application of AMS in the UDMA. We combine AMS with structural, petrographic and geochemical observations as a basis to relate the emplacement of the Tafresh granitoids (Sarbadan and Ghahan stocks) to developing tectonic stress/strain fields in Late Miocene time. AMS is used because fabric measurements in granites are rather difficult to obtain directly in the field (Bouchez, 1997). This enables us to constrain the kinematics of magmatism in the UDMA.

2. Regional geology

The Tafresh area (35.00°–34.30° N, 50.00°–50.30° E) within the central UDMA, located ∼180 km southwest of Tehran, occupies an area of ∼150 km^2. It contains plutonic, volcano-sedimentary and sub-volcanic units (Fig. 1b). The Sarbadan and Ghahan stocks were intruded into an Eocene volcano-sedimentary series. In map view, these shallow-level intrusions exhibit stretching in an E–W direction (Fig. 1b). The Sarbadan and Ghahan stocks are of Late Miocene age (respectively, 19.07 ± 0.25 Ma and 20.37 ± 0.41 Ma), based on U–Pb zircon data (McFarlane, pers. comm.). Based on field evidence (Fig. 2) and petrographic observations (Fig. 4), the stocks consist of granodiorite (Sarbadan) and diorite–quartz diorite (Ghahan). Outcrops of the Sarbadan stock are blocky to massive, covering an area of 20 km^2 extending in an E–W direction from northeast of Tafresh city to Ghahan village. This stock is in contact with younger pyroclastic units and a thick Eocene sequence of volcanic rocks (andesitic basalt, andesite, dacite). In these light grey host rocks, minerals visible in hand specimen are mainly hornblende, feldspar and quartz (Fig. 2a). Outcrop of the shallow-level Ghahan stock is in the form of a dome whose areal extent of ∼18 km^2 displays a marked W–E elongation. Grey to light grey Ghahan rocks are characterized by porphyritic to sub-granular textures in which hornblende and feldspar are prominent (Fig. 2b). These are enclosed by Eocene pyroclastic rocks, which include tuffs and dacitic to andesitic lavas. Microdioritic enclaves, occurring mainly in the coalescence zone between the Ghahan and Sarbadan stocks, vary from 5 to 10 cm and exhibit circular to ellipsoidal shapes (Fig. 2c). Regionally, the study area was affected by reverse and dextral faulting associated with thrusting of the Eocene volcano-sedimentary series over the Oligocene Qom Formation and Pliocene conglomerates (Hajian, 1977). Most faults are parallel to the regional tectonic fabric of the UDMA (e.g. the Tafresh, Indes, Tabarteh and Talkhab faults). The dominant trends are NW–SE, although subordinate fault and fracture systems with E–W and SW–NE trends are also common (Fig. 3). The mean strike of a Tafresh fault varies from N130 to N150W, with an average dip of 50° to the southwest. To the north and parallel to the Tafresh fault, the Indes fault of 120 km length has a similar geometry with a ∼75° dip to the southwest. To the south, and parallel to the Tafresh and Indes faults, the Talkhab fault dips ∼75° to the northeast (Morley *et al.* 2009). The Talkhab and Indes faults have both thrust and strike-slip movements (Rajabioun, 2000).

3. Methods

Oriented cylindrical cores were obtained from 31 sites: 15 granodiorite stations and 16 diorite–quartz diorite stations. Two or three oriented cores were collected per station, each yielding at least two samples, thus providing five (or more) samples per station. In all, 182 samples were analysed for magnetic parameters. All samples were sliced in order to obtain cylinders that fit in the sample holders of the Kappabridge instrument. Each sample was shaped to 22 mm length and 25 mm diameter: the standard size for magnetic measurements. Magnetic fabric was measured at the Geomagnetic Laboratory, Shahrood University of Technology, using an AGICO Kappabridge MFK1-FA susceptometer operating at low field (4×10^{-4} T; 920 Hz). Orientations and magnitudes

https://doi.org/10.1017/S0016756818000766 Published online by Cambridge University Press

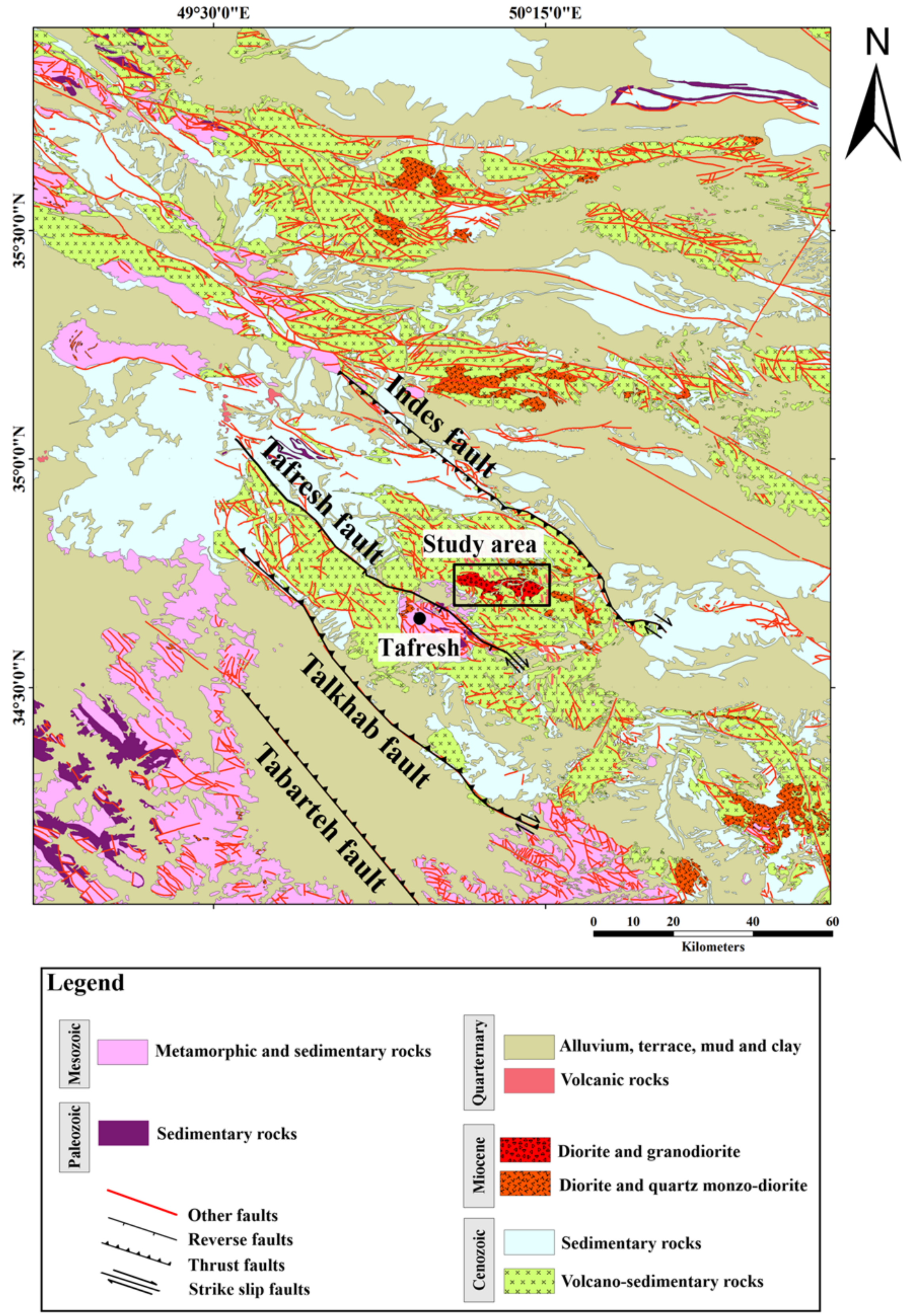

Fig. 3. (Colour online) Tectonic map of the Tafresh area showing the main faults. 1:250000 geological maps of Iran (www.gsi.ir).

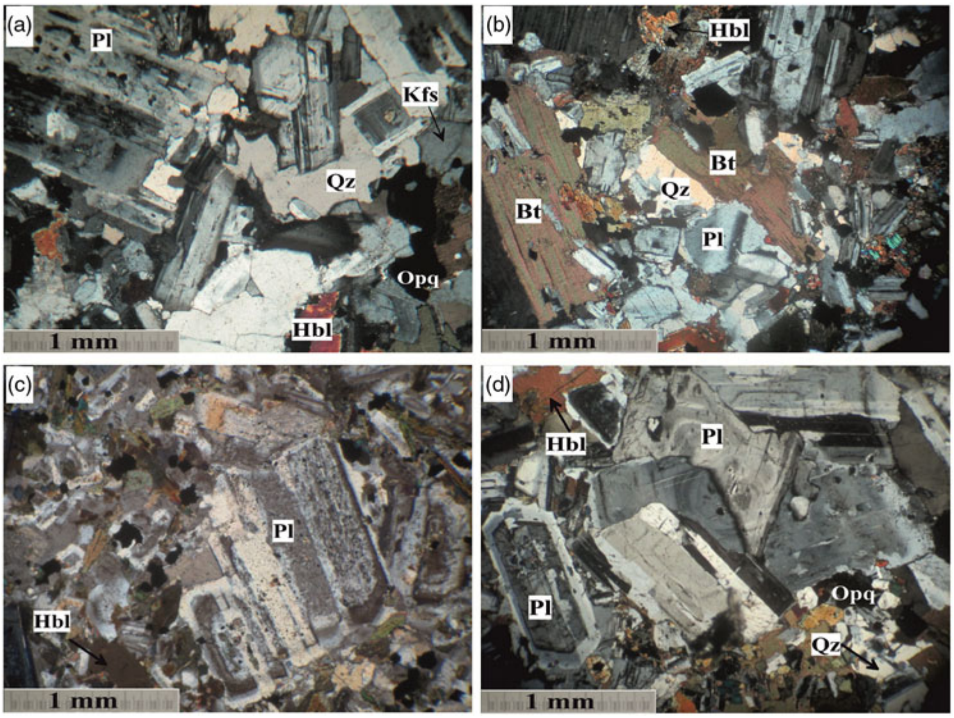

Fig. 4. (Colour online) Petrographic characteristics of different rocks from the Tafresh granitoids. (a, b) Granular to sub-granular granodiorite with plagioclase (Pl), quartz (Qz), K-feldspar (Kfs), biotite (Bt) and hornblende (Hbl) minerals, Sarbadan stock. (c) Sub-granular diorite containing plagioclase, hornblende and opaque minerals (Opq), Ghahan stock. (d) Euhedral plagioclase with oscillatory zoning, Ghahan stock. Mineral abbreviations after Whitney & Evans (2010).

of the three principal axes of the AMS ellipsoids ($K_1 \geq K_2 \geq K_3$) were obtained for each sampling station using the rotating mode. The long axis of the ellipsoid, K_1, defines the magnetic lineation; K_3, the short axis, defines the pole of the magnetic foliation (the plane formed by K_3 and K_2 axes). The anisotropy percentage $P\% = 100((K_1/K_3) - 1)$ and the shape parameter $T = \ln(K_2/(K_1/K_3))/\ln(K_1/K_3)$ (Jelínek & Kropáček, 1978) were calculated for each sampling station. Table 1 records magnetic data for each of the 31 stations.

Electron microprobe analysis of magnetite grains was accomplished at the Iranian Mineral Processing Research Centre using a Cameca SX 100 electron microprobe analyser equipped with a wavelength-dispersive spectrometer. Accelerating voltage was 15 kV, with a beam current of 20 nA and a 0–2 µm focused electron beam. Table 2 provides representative magnetite analyses.

Fifty-one thin-sections were examined by optical microscopy, and ten representative fresh samples of intrusive rocks in the region were selected for whole-rock geochemical analysis. Major and trace elements were measured using inductively coupled plasma optical emission spectrometry (ICP-OES) and inductively coupled plasma mass spectrometry (ICP-MS), respectively, at the Department of Geology and Environmental Earth Sciences, Miami University, Ohio (Table 3). Two kilograms of each sample were powdered, and analyses were obtained by fusing 50 mg of sample powder with 75 mg $LiBO_2$ and dissolving in 125 ml of 0.3N HNO_3. For major elements, analytical precision is better than ± 2–5 %; for most trace elements and rare earth elements (REEs), the analytical error was less than 2 % and the precision was greater than 10 %.

4. Petrography and geochemistry

Sarbadan granodiorite has a medium-grained granular texture (Fig. 4a, b) and consists of plagioclase, K-feldspar, quartz, biotite and hornblende. Opaque minerals, pyroxene, zircon and titanite are conspicuous accessory minerals. Plagioclase forms euhedral to subhedral and tabular crystals (2.7 to 0.2 mm) with optical zonation. Most of the quartz occurs as small interstitial grains (0.1 to 0.64 mm). Opaque minerals (mainly magnetite), as inclusions in plagioclase or as forming small grains in the groundmass, occur mainly around the hornblende and biotite (Fig. 4b).

Ghahan diorite to quartz diorite has a granular to porphyritic texture with a microgranular groundmass (Fig. 4c). Plagioclase, K-feldspar and hornblende constitute the essential rock-forming minerals, whereas quartz ± biotite and opaque minerals, zircon and titanite form the accessory minerals. Plagioclase is euhedral to subhedral and commonly shows compositional zoning (Fig. 4d).

In the TiO_2–Fe_2O_3–FeO diagram, the opaque minerals of the Ghahan and Sarbadan stocks plot within the field of magnetite (Fig. 5). SiO_2 in the Ghahan stock is lower (SiO_2 = 58.58–60.82 wt %) than SiO_2 in the Sarbadan stock (SiO_2 = 62.77–65.07 wt %). According to the $K_2O + Na_2O$ versus SiO_2 diagram of Middlemost (1991), the analysed samples are classified as diorite (Ghahan) and granodiorite (Sarbadan) (Fig. 6a). The data define a calc-alkaline trend on the AFM diagram (Fig. 6b). A/CNK ((Al_2O_3/(CaO + Na_2O + K_2O)) ranges between 0.75 (Ghahan) and 0.96 (Sarbadan), indicating metaluminous magma (Fig. 7a). On the Na_2O versus K_2O diagram, samples are classified as I-type granitoids (Fig. 7b). On the plot of FeO_t/MgO versus Zr + Nb + Ce + Y (Whalen *et al.* 1987), all data correspond to unfractionated I- and S-type granitoids (Fig. 7c). Trace-element discrimination diagrams can be employed as a means to 'fingerprint' the tectonic environments in which granitoids formed (Pearce *et al.* 1984). Accordingly, in a plot of Rb versus Ta + Yb, all samples correspond to volcanic arc granitoids (Fig. 7d). A high Rb/Nb ratio, between 1.56 and 12.62, is consistent with a subduction zone setting (Pearce, 1983). Harker diagrams (Fig. 8) exhibit ascending linear trends for Na_2O, but negative trends for TiO_2, Al_2O_3, FeO, MnO and CaO, suggestive of fractionation of amphibole, biotite and magnetite. K_2O versus SiO_2 is positive, and K_2O versus SiO_2 does not show a clear trend.

https://doi.org/10.1017/S0016756818000766 Published online by Cambridge University Press

Table 1. Anisotropy of magnetic susceptibility data for the Ghahan and Sarbadan stocks

				Mean AMS parameters			Mean eigenvectors					
							K1		K2		K3	
Station	N	X	Y	Km (μSI)	P%	T	Decl	Incl	Dec	Incl	Decl	Incl
G1	6	427961	3842796	9846	6.0	−0.30	166.80	9.90	267.24	45.88	67.76	42.26
G2	6	428296	3842504	12966	5.2	−0.47	204.76	16.69	193.11	30.56	113.87	53.27
G3	5	428285	3841867	5815	7.1	0.34	140.76	64.58	160.62	17.11	230.49	13.83
G4	6	428974	3841424	12921	3.4	0.71	214.30	42.84	204.48	40.98	134.82	15.60
G6	6	430055	3841862	19785	2.2	−0.09	85.37	86.59	154.93	2.84	167.79	1.07
G7	7	430912	3841518	23564	2.1	−0.41	204.96	42.52	92.08	43.78	231.34	10.76
G8	5	427412	3844124	5620	9.4	0.02	265.38	59.70	143.95	20.38	141.83	18.88
G11	5	423201	3843246	26341	4.2	0.25	209.83	80.43	131.97	8.93	161.57	3.03
G12	6	430481	3842256	23590	2.5	0.29	110.64	66.74	296.64	22.10	204.52	6.40
G13	6	429261	3842143	27175	3.1	−0.47	177.26	65.70	122.12	20.88	312.66	7.08
G14	6	428083	3840826	9021	1.2	0.45	258.42	73.14	88.38	16.68	213.80	1.90
G16	7	427508	3841774	22384	6.2	0.33	343.10	39.75	168.85	46.60	159.20	13.60
G17	6	426854	3843604	15820	3.2	−0.09	148.94	35.04	122.12	28.14	231.00	37.34
G20	6	426538	3840663	17576	1.7	0.31	208.75	19.20	206.05	40.58	110.33	41.50
G21	6	426554	3841966	16679	2.4	−0.28	109.54	32.52	226.04	47.96	144.22	17.80
G22	6	425576	3843153	56387	2.0	0.00	159.34	36.94	123.06	47.32	294.32	13.66
S1	6	417248	3842584	11486	7.1	0.14	191.33	27.98	280.15	17.85	139.78	51.67
S2	5	418322	3845101	36394	2.3	0.22	109.35	63.63	284.10	24.60	105.03	8.58
S3	6	417731	3844646	23809	2.1	−0.48	134.93	76.68	230.93	8.98	185.65	7.65
S4	6	416869	3843916	31856	6.0	0.40	203.10	7.53	135.33	74.97	171.93	12.20
S5	7	415266	3843458	17271	5.3	0.71	229.26	25.18	94.40	40.70	202.48	32.84
S6	7	420929	3843612	65476	8.0	0.33	162.50	69.65	274.95	18.73	182.75	6.90
S7	6	422309	3843193	46733	3.9	0.33	144.93	25.57	226.37	44.03	183.13	33.63
S8	6	422131	3844267	40361	4.4	0.25	147.33	25.24	133.10	34.03	272.16	41.71
S9	6	420333	3844282	12975	1.6	0.29	115.83	12.10	208.55	11.03	248.48	73.48
S10	5	419517	3844383	71591	7.3	0.62	244.56	5.27	181.14	13.04	131.41	75.23
S13	5	419673	3842841	48111	9.9	0.74	203.18	16.78	216.45	39.02	125.42	43.87
S14	5	419603	3841949	43187	6.2	0.62	160.35	22.93	254.50	12.03	191.75	61.47
S15	5	418626	3841793	33592	8.7	0.40	105.03	15.20	158.96	33.86	212.69	49.19
S16	6	419778	3841157	32879	11.4	0.73	151.88	19.50	36.48	48.00	254.53	33.83
S17	6	420838	3841451	43542	5.1	0.32	143.24	48.48	32.64	18.24	288.92	34.50

Locations (X (x-coordinate) / Y (y-coordinate) in Universal Transverse Mercator (UTM) zone; Km = $(K_1 + K_2 + K_3)/3$ mean magnetic susceptibility in 10^{-6} SI; P% = $100 \times ((K_1/K_3) - 1)$ is the total anisotropy percentage; T = $(2\ln(K_2/K_3)/(\ln(K_1/K_3) - 1)$ is the Jelinek's shape parameter (Jelínek, 1981). Decl – declination; Incl – inclination in degrees.

Chondrite-normalized REE patterns (Sun & McDonough, 1989) show relative enrichment of light rare earth elements (LREE), and relatively flat heavy rare earth element (HREE) patterns, with an absent Eu anomaly (Fig. 9a). On a multi-element diagram normalized to primitive mantle (Sun & McDonough, 1989), Nb, P and Ti show distinctly negative anomalies, whereas large-ion lithophile elements (LILEs, such as Cs, Rb, K and Pb) exhibit pronounced positive anomalies (Fig. 9b).

5. Magnetic fabric

The AMS technique provides a rapid quantitative description of the crystal shape fabric in magmatic rocks (e.g. Gleizes *et al.* 1993; Cruden & Launeau, 1994; Bouchez, 1997; Cruden *et al.* 1999; De Saint-Blanquat *et al.* 2001; Cañón-Tapia & Coe, 2002; Cañón-Tapia & Chávez-Álvarez, 2004; Archanjo & Launeau, 2004; Eriksson *et al.* 2011; Archanjo *et al.* 2012; Schöpa *et al.* 2015). It also helps in determining the bulk internal structure of plutons in situations where macroscopic foliation and lineation are weak or absent (Sheibi *et al.* 2012). In anisotropic rocks, the magnetic susceptibility is represented by a second-order symmetric tensor, an ellipsoid with three principal susceptibility axes (Bouchez, 2000). The relationship between preferred mineral orientation and magnetic fabric depends on the nature of the magnetic minerals, and on the textural relationships among the mineral grains (Stacey, 1962; Khan, 1962; Uyeda *et al.* 1963; Rochette *et al.* 1992;

https://doi.org/10.1017/S0016756818000766 Published online by Cambridge University Press

Table 2. Selected electron microprobe analyses of magnetites from the Tafresh granitoids

Point. No	T1	T2	T3	T4
SiO_2	0.040	0.030	0.080	0.020
TiO_2	0.230	0.080	0.130	0.140
Al_2O_3	0.120	0.000	0.500	0.290
FeO	92.720	91.880	92.600	90.960
MnO	0.090	0.060	0.010	0.000
CaO	0.020	0.020	0.010	0.030
Na_2O	0.110	0.080	0.000	0.100
K_2O	0.020	0.000	0.000	0.010
P_2O_5	0.020	0.000	0.040	0.000
Total	93.370	92.150	93.370	91.550
Si	0.012	0.009	0.025	0.006
Ti	0.053	0.019	0.030	0.033
Al	0.044	0.000	0.181	0.107
Fe(iii)	15.825	15.944	15.710	15.814
Fe(ii)	8.035	8.006	8.049	8.029
Mn	0.023	0.016	0.003	0.000
Ca	0.007	0.007	0.003	0.010
Fe_2O_3	68.340	67.975	68.045	67.044
FeO	31.225	30.713	31.370	30.630

De Saint-Blanquat *et al.* 2006). Maximum, intermediate and minimum susceptibilities are designated as $Kmax = K_1 > Kint = K_2 > Kmin = K_3$, respectively, representing the maximum, intermediate and minimum axes of the magnetic susceptibility ellipsoid. The ellipsoid long axis, K_1, defines the magnetic lineation and the short axis, K_3, defines the pole to the magnetic foliation (Tcheumenak Kouémo *et al.* 2014). Magnetic lineation (K_1) is often inferred to indicate the stretching direction of magmatic flow (Owens, 1974; Guillet *et al.* 1983; Bouchez *et al.* 1990; Bouchez, 1997; Cañón-Tapia *et al.* 1997; Bella Nké *et al.* 2014). The average value of $Km = 1/3(K_1 + K_2 + K_3)$, known as the bulk susceptibility, varies according to the relative proportions of ferromagnetic, paramagnetic and diamagnetic minerals present in the rock (Tarling & Hrouda, 1993). The intensity of anisotropy (degree of eccentricity) of the AMS ellipsoid is studied through P% (Jelínek, 1981). The shape of the AMS ellipsoid is illustrated by the T parameter, which varies from +1 for a perfectly oblate ellipsoid to −1 for a perfectly prolate ellipsoid (Jelínek, 1981).

5.a. Bulk magnetic susceptibility (Km)

The classic subdivision into 'paramagnetic' and 'ferromagnetic' granites was recognized early on by Ishihara (1977) in order to sort Japanese granites into magnetite-absent and magnetite-bearing facies, as evidenced by low-field magnetic susceptibility and anisotropy measurements, respectively. In magnetite-absent granites, the susceptibility carriers are the iron-bearing silicates (i.e. biotite, chlorite, amphibole, tourmaline, etc) and Km does not exceed 0.5×10^{-3} SI. In the ferromagnetic type, the presence of magnetite in addition to the iron-bearing silicates is responsible for high Km ($>5 \times 10^{-3}$ SI). Since magnetite has a strong intrinsic susceptibility, the added effect of the paramagnetic and diamagnetic minerals is modest and the magnetic susceptibility of a rock is largely controlled by the magnetite content (Gleizes *et al.* 1993; Bouchez, 1997). The magnetic susceptibility varies from 11.5×10^{-3} SI (station S1) to 71.6×10^{-3} SI (station S10) (mean value 37.3×10^{-3} SI) for Sarbadan, and 5.6×10^{-3} SI (station G8) to 56.4×10^{-3} SI (station G22) (mean value 19.1×10^{-3} SI) for Ghahan (Figs 10, 11). Susceptibility is highly variable across the stocks, and the average bulk magnetic susceptibility of the Sarbadan stock is higher than that of the Ghahan.

5.b. Magnetic anisotropy percentage (P%)

Since the anisotropy percentage is usually related to the intensity of deformation, this parameter is often used to distinguish magmatic flow from solid-state deformation (De Saint-Blanquat *et al.* 2001). In some cases, P% may be correlated with strain intensity (Bouchez, 1997). P% is equal to 1 when $K_1 = K_2 = K_3$ and the magnetic ellipsoid is a sphere. In any case, an increase in the magnetic susceptibility results in augmenting the differences among the axes and resultant degree of anisotropy. AMS depends upon several factors such as temperature, deformation and chemical composition of rocks, etc (Bouchez, 2000). The measured P% for the Sarbadan and Ghahan stocks (Table 1) is shown as contours in Figure 12a. P% is low throughout the pluton, varying from 1 % to 11 % (mean 4.74 %), rarely exceeding 10 %. High values of P% are located at sites on the southern margin of the Sarbadan stock. Occasional undulose extinction in quartz and minor mechanical twining in plagioclase are the only evidence of solid-state deformation in the western margin of the Ghahan stock. Owing to the subgranular texture of the two stocks, it is possible that traces of deformation are not recorded.

5.c. Shape parameter (T)

The magnetic shape parameter (T) characterizes the shape of the magnetic susceptibility ellipsoid (Jelínek, 1981; Borradaile, 1988) and delineates the direction and arrangement of the magnetite crystals during emplacement (Jelínek & Kropáček, 1978). If T is negative, the shape of the magnetic ellipsoid is prolate or linear, whereas for positive T the ellipsoid is oblate or disc shaped (Lanza & Meloni, 2006). Shape parameters for the Sarbadan and Ghahan stocks range from −0.48 (station S3) to 0.74 (station S13) and −0.47 (station G2) to 0.71 (station G4), respectively (Fig. 12b). Stations with negative values may represent the locus of feeder zones.

A plot of P% and T versus Km has been used in AMS studies to correlate specific shape fabrics with either susceptibility or anisotropy. Figure 13a, b shows P% versus Km and T versus Km, respectively. The relationship between P% and Km suggests the Sarbadan stock is both richer in magnetite and more deformed (Fig. 13a). No apparent correlation exists between T versus Km (Fig. 13b), but most stations of the Sarbadan stock are in the domain of an oblate ellipsoid, and 44 % of stations of the Ghahan granitoid are in the domain of a prolate-shaped ellipsoid. The T versus P% diagram reveals that the ellipsoids show a priority from oblate to prolate (Fig. 13c).

5.d. Patterns of magnetic fabrics

Mineral lineations are crucial in understanding flow mechanism and emplacement history. Figure 14a, b displays magnetic

https://doi.org/10.1017/S0016756818000766 Published online by Cambridge University Press

Table 3. Major (wt %), trace and rare earth element (ppm) data of representative rock samples from the Tafresh granitoids

Rock type	Granodiorite				Diorite					
Sample	S1	S2	S3	S4	G1	G2	G3	G4	G5	G6
SiO_2	63.55	63.26	62.77	65.07	59.68	59.41	58.59	59.48	60.36	60.83
TiO_2	0.57	0.58	0.59	0.56	0.53	0.68	0.65	0.60	0.60	0.40
Al_2O_3	16.73	16.36	16.42	16.73	17.38	18.39	17.93	17.43	17.75	16.66
FeO(t)	4.92	5.33	5.18	4.32	4.35	5.95	5.95	5.44	5.49	5.54
MnO	0.10	0.13	0.13	0.11	0.11	0.12	0.12	0.12	0.12	0.06
MgO	2.21	2.27	2.16	2.78	2.78	2.61	2.55	2.64	2.73	2.60
CaO	5.67	5.64	5.52	4.88	7.67	7.44	7.31	6.79	7.04	5.14
Na_2O	3.54	3.85	3.83	2.98	3.98	3.94	3.85	3.54	3.66	3.89
K_2O	1.82	2.19	2.17	1.63	0.23	0.94	0.89	1.16	1.16	2.06
P_2O_5	0.12	0.13	0.12	0.18	0.13	0.14	0.14	0.10	0.11	0.09
LOI	1.77	1.27	0.64	1.85	2.47	0.97	1.65	1.94	0.37	1.84
Total	101.00	101.00	99.53	101.10	99.30	100.60	99.65	99.24	99.39	99.10
Cs	1.59	1.37	0.50	2.00	0.12	0.20	0.19	0.84	0.31	0.53
Rb	61.85	63.99	56.50	36.12	6.12	19.21	17.21	17.18	27.38	35.82
Ba	486.19	482.28	486.06	462.00	139.83	388.35	376.29	390.35	394.02	623.77
Th	5.25	8.26	8.61	4.22	5.12	2.82	2.47	2.05	3.81	5.97
U	1.51	2.17	3.34	0.70	0.80	1.27	1.26	0.68	1.61	2.87
Nb	4.90	6.54	5.02	4.10	3.92	4.46	5.12	2.95	3.25	5.40
Ta	0.55	0.50	0.43	0.41	0.41	0.30	0.28	0.28	0.32	0.41
La	21.90	13.34	16.19	12.00	12.45	9.72	9.24	11.66	11.32	9.50
Ce	43.18	29.60	31.14	25.00	19.25	21.98	20.82	17.61	19.33	22.72
Pb	10.77	11.57	4.21	11.00	0.45	7.36	10.54	9.10	12.57	10.41
Sr	264.99	370.10	358.64	225.40	525.24	453.10	443.82	424.22	445.19	329.15
P	530.89	585.62	534.70	345.02	548.70	632.40	631.89	420.18	479.11	385.91
Nd	16.86	15.68	7.21	12.60	6.11	15.18	14.24	3.89	13.46	6.58
Hf	2.83	3.90	5.32	0.40	3.84	3.27	2.52	2.61	1.16	1.84
Zr	126.62	162.04	175.55	7.00	108.84	153.91	129.79	58.60	68.42	106.60
Sm	2.19	3.03	2.19	2.46	1.68	1.63	1.50	0.78	0.99	1.65
Tb	0.48	0.53	0.38	0.44	0.51	0.52	0.50	0.54	0.44	0.36
Y	18.31	22.15	19.27	14.60	18.34	20.85	20.42	14.97	17.69	13.48
Er	2.05	3.59	1.49	1.67	0.80	1.31	2.32	0.62	0.75	0.69
Tm	0.25	0.32	0.19	0.22	0.30	0.29	0.28	0.30	0.24	0.19
Yb	1.73	2.23	2.46	2.00	2.23	2.09	2.03	2.04	1.75	1.16
Co	33.07	12.66	14.19	14.00	13.44	13.92	12.14	16.28	13.74	5.93
Cr	22.98	27.89	19.54	10.00	7.03	17.37	16.17	15.32	17.95	33.19
Cu	6.62	24.53	23.07	22.00	2.08	7.52	6.53	35.90	39.79	4.12
Dy	2.73	3.24	1.91	2.81	1.89	3.35	2.95	1.13	1.71	2.03
Mo	0.22	1.25	1.54	0.10	1.36	0.77	0.98	0.59	1.22	0.68
Ni	62.82	109.42	49.97	3.00	6.19	106.77	18.48	9.16	13.94	137.51
Sc	11.41	11.37	10.54	11.20	13.89	13.30	13.10	13.00	13.76	7.86
V	103.57	118.39	110.48	110.00	122.80	133.58	134.53	138.87	137.82	81.02
Zn	44.60	46.07	38.86	52.00	42.62	34.78	28.47	22.98	36.19	20.60
Ga	16.24	15.16	12.83	16.24	15.65	17.25	16.97	15.23	16.56	13.02
As	0.49	1.39	1.15	9.50	6.00	−0.07	−0.01	4.95	0.15	0.84

(*Continued*)

https://doi.org/10.1017/S0016756818000766 Published online by Cambridge University Press

Table 3. (*Continued*)

Rock type	Granodiorite				Diorite					
Sample	S1	S2	S3	S4	G1	G2	G3	G4	G5	G6
Sn	0.90	1.06	1.04	1.00	0.68	0.95	0.92	0.76	0.99	0.99
Sb	0.90	1.04	1.00	0.43	0.35	0.88	0.97	0.08	0.94	0.94
Pr	4.79	3.73	3.05	3.06	2.92	3.13	3.07	2.80	2.96	3.07
Eu	0.95	1.05	1.14	0.76	1.14	1.14	1.10	1.10	0.94	0.73
Gd	3.22	3.41	2.33	2.07	3.04	3.26	3.19	3.19	2.78	2.21
Dy	2.58	3.10	1.90	2.66	3.03	2.98	2.86	3.29	2.45	1.85
Ho	0.61	0.75	0.47	0.63	0.68	0.71	0.69	0.71	0.59	0.46
Lu	0.26	0.33	0.21	0.25	0.32	0.30	0.28	0.32	0.25	0.20
A/CNK	0.92	0.86	0.88	0.75	0.84	0.87	0.87	0.90	0.88	0.91
A/NK	2.15	1.88	1.90	1.76	2.56	2.45	2.46	2.46	2.44	1.70

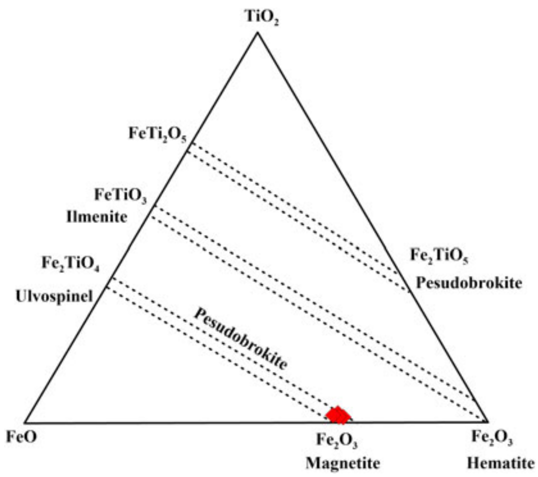

Fig. 5. (Colour online) Chemical composition of magnetite on TiO_2–Fe_2O_3–FeO ternary diagram (Buddington & Lindsley, 1964).

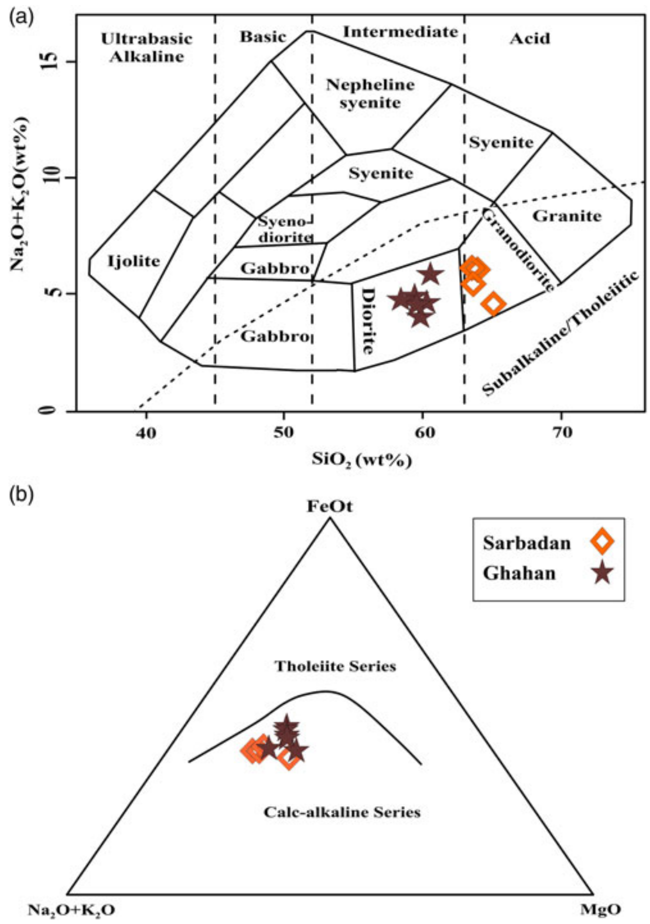

Fig. 6. (Colour online) Chemical classification of rocks from the Ghahan and Sarbadan stocks. (a) $K_2O + Na_2O$ v. SiO_2 plot (Middlemost, 1991); composition of studied samples ranges from diorite (Ghahan stock) to granodiorite (Sarbadan stock). (b) AFM ($A = Na_2O + K_2O$; $F = FeO_t$; $M = MgO$) diagram with differentiation lines of Irvine & Barager (1971), showing a calc-alkaline affinity for the granitoids (Irvine & Baragar, 1971).

lineation and foliation maps for the Tafresh granitoids, and stereo-plots of the foliation and lineation poles. In general, the magnetic lineations are radially distributed from steep to gentle plunges from north to south in each stock. It is evident from the geometry of the lineation trajectories that the magma flowed outward radially from the northern entry point, towards the southern margins. In stereo-plots, the magnetic lineations are widely spread (Fig. 14a, b). The average trend/plunge of magnetic lineation in the Sarbadan and Ghahan stocks is 142°/36° and 205°/48°, respectively (Fig. 14a). Seven stations having steep lineation plunges (>60°) are considered to be probable feeder zones. In 11 of the stations, magnetic foliation dips are greater than 70° with various strikes. The average foliation poles for the Sarbadan and Ghahan stocks are 221°/58° and 128°/30°, respectively (Fig. 14b). Most of the magnetic foliations are vertical or close to vertical, outlining a circular pattern on the Earth's surface.

6. Discussion

6.a. Constraint on petrogenesis

The Tafresh granitoids have arc-like, calc-alkaline signatures with similar REE patterns (especially in the HREEs), with Nb, Ta, Ti and Ba depletion, and with LREE and LILE enrichment (Fig. 9). Although negative anomalies in high field strength elements (HFSEs) might be linked to crustal contamination, we favour an interpretation that these anomalies typify subduction-related

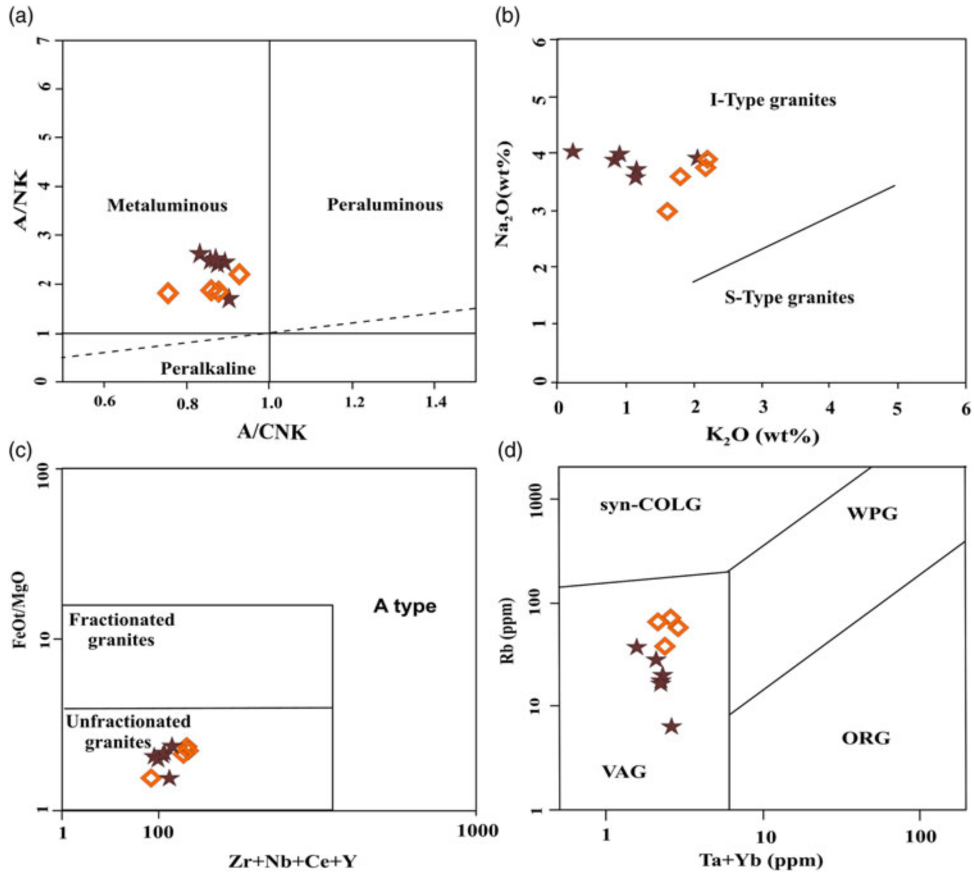

Fig. 7. (Colour online) (a) Classification of the Ghahan and Sarbadan stocks on A/NK v. A/CNK diagram (ANK = molar $Al_2O_3/(Na_2O + K_2O)$ and ACNK = molar $Al_2O_3/(CaO + Na_2O + K_2O)$) (Shand, 1943). (b) Na_2O v. K_2O classification diagram for discrimination of I- and S-type granitoids (Chappell & White, 2001); all samples fall in the field of I-type granitoids. (c) FeO_t/MgO v. Zr + Nb + Ce + Y diagram. (d) Tectonic classification diagram Rb v. Ta + Yb (Pearce *et al.* 1984). WPG – within-plate granites; VAG – volcanic arc granites; syn-COLG – syn-collision granites; ORG – oceanic ridge granites.

magmas; they originate from LILE enrichment in the subducting slab (Borg *et al.* 1997). The Nb–Ta trough is considered to characterize arc-related I-type granitoids (e.g. Rogers & Hawkesworth, 1989; Sajona *et al.* 1996). On the chondrite-normalized diagram, the samples are LREE-enriched relative to enrichment in middle rare earth elements (MREE) and HREEs, but with relatively flat or upward-sloping MREE–HREE patterns, and with Eu anomalies absent. Second-order variations in LREE enrichment could be attributed to varying source compositions or degree of partial melting (Langmuir *et al.* 1977; Le Roex, 1987; Kamenetsky *et al.* 2000). The absence of negative Eu anomalies can be ascribed to the oxidizing conditions, such that Eu is present as Eu^{3+}, and not Eu^{2+}. The common occurrence of magnetite (Fig. 5) and hornblende in the Tafresh intrusive rocks indicates a high oxidation state and elevated water contents of the parent magmas (Hanson, 1980), which likely explains the lack of a distinct Eu anomaly. The profiles of REEs and the unfractionated HREE (and Y) patterns (Fig. 9) suggest that the magmas were produced outside the garnet stability field, likely in an amphibole-bearing mantle source, overlain by a relatively thin crust. On the tectonic discrimination diagram of Pearce *et al.* (1984) (Fig. 7d), all sample data fall in the domain of volcanic arc granitoids.

6.b. Emplacement model

Petrological studies and the results obtained from the AMS methodology indicate that the Sarbadan and Ghahan stocks are I-type, ferromagnetic granitoids emplaced at shallow crustal depth in the central part of the UDMA. The two stocks share genetic relationships imposed during a single tectonic event. Microstructural analyses and consistently low anisotropy values across the Ghahan and Sarbadan stocks point to the dominance of magmatic flow rather than solid-state deformation. Occasional occurrence of weak solid-state deformation within the western margin of the Ghahan stock, the presence of microdioritic enclaves in the zone of convergence of these two stocks, the growth and southward expansion of the stocks and similar U–Pb ages all point to the coalescence of two magma chambers. The magnetic fabric of the Ghahan and Sarbadan stocks was created with a circular pattern and vertical foliation, and a high-dip lineation with a gradual distribution from an almost E–W vertical foliation and a horizontal southward lineation. In each stock, a distinct feeder zone with a steep magnetic lineation plunge (>60°) suggests that magma ascended dominantly along a NW–SE direction. Feeder zones are tentatively identified as being tectonically developed in extensional gashes. In separated feeder zones, magma conduits formed in the lower parts of a brittle crust. According to recent studies, most plutons are not ‘big-tank’ magma chambers but, rather, they are constructed by amalgamation of small magma pulses (Glazner *et al.* 2004; Sheibi *et al.* 2012). For the Sarbadan and Ghahan granitoids, the E–W trend was located in a shear zone developed between the Indes and Talkhab faults (Fig. 15a). Minimum stresses, which are perpendicular to the main stress, act in a tensional manner. At Tafresh, the main NE–SW stress was parallel to the compression of Eurasian–Arabian block convergence (Fig. 15b). In this regard, we suggest that the Sarbadan and Ghahan granitoids were emplaced in a shear zone during an extensional opening phase. Evidence such as the pattern of

https://doi.org/10.1017/S0016756818000766 Published online by Cambridge University Press

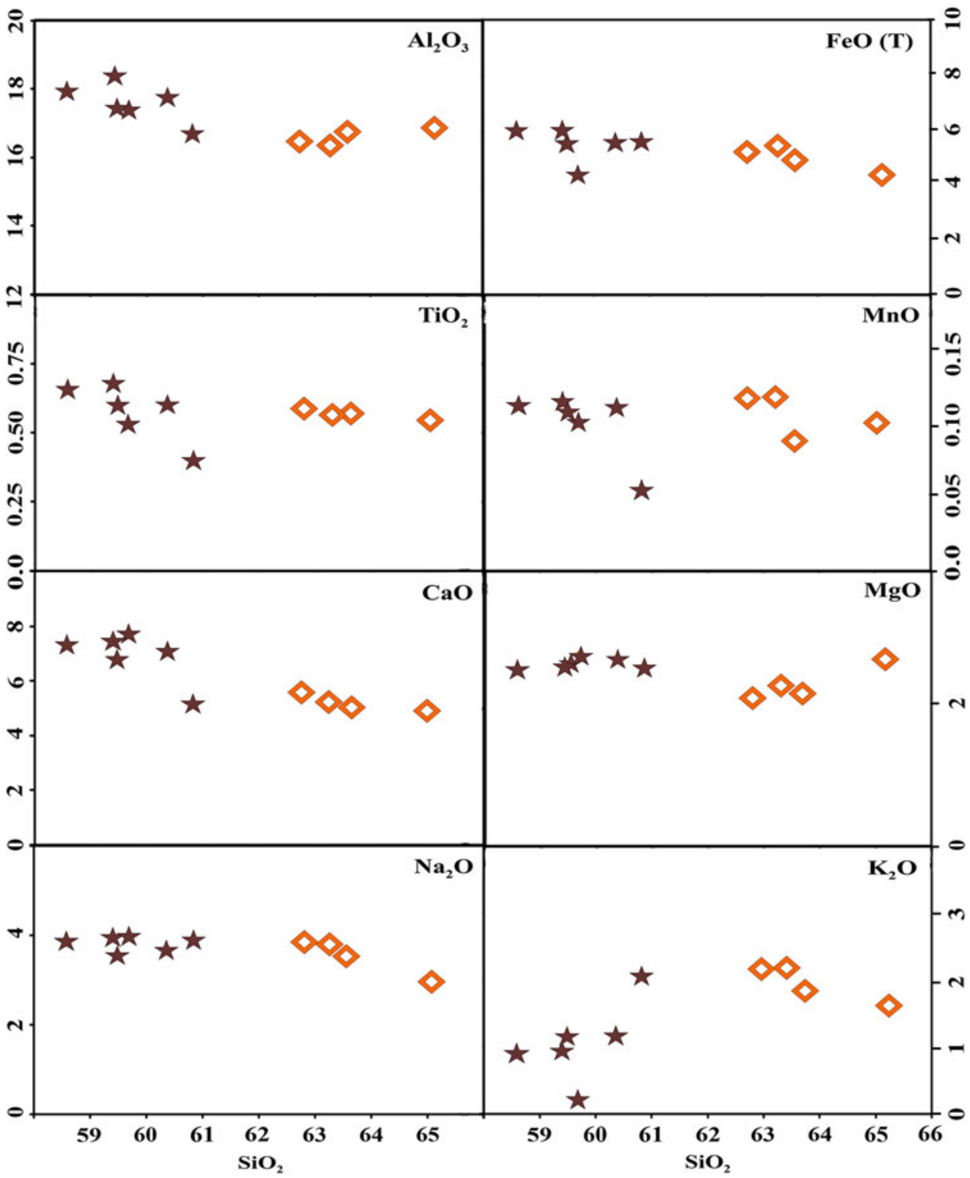

Fig. 8. (Colour online) Harker diagrams for major elements of the Tafresh granitoids.

emplacement of the Ghahan and Sarbadan stocks indicates that the main stress in the study area had a NE–SW trend and is parallel to the compressional stress induced by Eurasian–Arabian block convergence. Therefore, the Indes and Talkhab faults in Miocene time were active by left-lateral strike-slip movement (Fig. 15b). Coming back to the geological context and the AMS results obtained from the present study, we infer that the dextral shear zone tectonics in the UDMA might have given rise to local extensional voids or tensional gashes, into which the magma was emplaced. A simple shearing system created trends of individual plutons that are similar to the trend of widespread UDMA magmatism. We infer that the younger, more fractionated Sarbadan stock was emplaced later than the older, less fractionated Ghahan stock.

6.c. Structural significance

Structural investigation and modelling suggest a direct relationship between magma movement and emplacement along strike-slip (Corti *et al.* 2005), tensional (Hutton, 1988), transpressional (De Saint-Blanquat *et al.* 1998) and transtensional (Guineberteau *et al.* 1987) faults. Study of internal fabrics of plutonic complexes provides insight into regional tectonics, since magmatism can be associated with both compressional and extensional phases of an orogeny (Brown & Solar, 1998; De Saint-Blanquat *et al.* 1998).

Iran is located within the convergence domain between the Arabian and Eurasian plates (Regard *et al.* 2005). Movement of the Arabian plate was directed approximately N–S to N010E on average, relative to Eurasia (Masson *et al.* 2007; Agard *et al.* 2011). Shortening occurred in a SW–NE direction across the orogen during Mesozoic and Cenozoic times. Convergence between Arabia–Eurasia resulted in NW-trending parallel tectono-metamorphic and magmatic belts, among these being the SSZ and the UDMA (Berberian & Berberian, 1981; Berberian & King, 1981; Berberian *et al.* 1982). Subduction of the Neo-Tethys oceanic plate beneath the Eurasian plate was accompanied by Triassic–Jurassic Andean-like arc magmatism in the SSZ that had therefore been active at least 150 Ma prior to collision. The NW-trending SSZ, one of the youngest continental collision zones on Earth, is characterized by an extensive magmatic history. The collision

https://doi.org/10.1017/S0016756818000766 Published online by Cambridge University Press

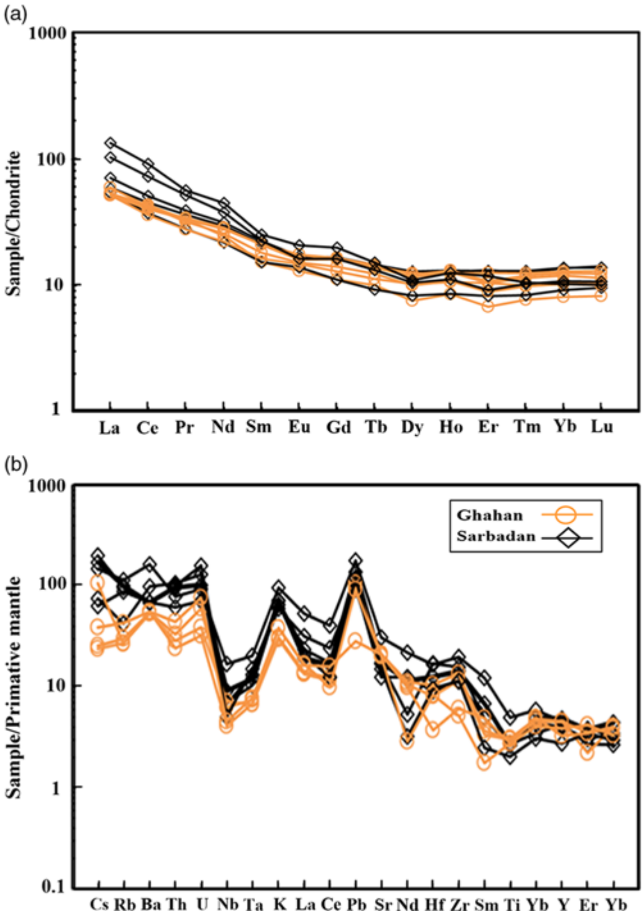

Fig. 9. (Colour online) (a) Chondrite-normalized REE patterns. Normalized values from Sun & McDonough (1989). (b) Primitive mantle normalized multi-element diagram. Normalizing values are after McDonough & Sun (1995).

occurred during closure of the Neo-Tethys Ocean between the Arabian and Eurasian plates (Berberian, 1995; Golonka, 2004).

T versus P%, T versus Km, and Frequency versus Km plots on the different granitoids from Iran are shown in Figure 16. Compilations of AMS data for Iranian granitoids (Table 4) show that although the plutons differ in age and structural and magmatic type, they are emplaced by similar mechanisms. Strike-slip movements within or close to most of the oblique magmatic arcs and contraction structures are often found in fore-arc and back-arc environments (De Saint-Blanquat *et al.* 2001). Strike-slip faulting is observed in many volcanic structures of magmatic arcs (Beck, 1983). In central Andean arcs (Mégard, 1987) and Japan (Lallemand & Jolivet, 1986), for example, strike-slip deformation occurs on the surface. Strike-slip tectonics can be associated with a subduction zone in two ways: (1) the linear trend parallel to the margin of the magmatic arc, and (2) high heat flow in an arc due to magma transfer that forms a weak zone along with the continental lithosphere (Jarrard, 1986). Shear displacements indicate the intensity and importance of regional fractures and associated magmatism.

7. Conclusions

(1) Sub-intrusive and intrusive rocks of the diorite–quartz diorite Sarbadan and granodiorite Ghahan stocks in the Tafresh area show porphyritic, granular to sub-granular textures. Enriched LREE patterns, high abundances of LILEs and depletion in HFSEs with significant negative Nb and Ta anomalies suggest that Early Miocene magma at Tafresh formed during subduction activity.

(2) High values of the Km (>5 × 10^{-3} SI) and geochemical data indicate that the Tafresh stocks are classified as ferromagnetic and I-type granitoids.

(3) Magnetic lineations indicate that each stock contains distinct feeder zones that were opened as a consequence of extension.

(4) Magnetic data and structural evidence show that shear zones had caused an opening, facilitating consequent migration, ascent and emplacement of granitoid magmas in the Tafresh area during an extensional phase.

(5) The E–W trend of the Sarbadan and Ghahan stocks and their emplacement in the middle part of the UDMA developed between the Indes fault and Talkhab fault as a product of tensional stress in a brittle tectonic regime, ancillary to compressional stresses induced by Eurasian–Arabian block convergence.

(6) Compilation of several studies dealing with mechanisms of magma emplacement in Iran confirms that magma was emplaced during a transpressive to transtensional episode during oblique subduction of the western Neo-Tethys beneath central Iran. Structural investigation of these studies emphasizes a direct relationship between the faults and magma movements and emplacement along strike-slip faults. This shear deformation along the main faults of Iran can be attributed to the convergence between the major Arabian–Eurasian continental blocks.

Acknowledgements. Dear Prof. Jean Luc Bouchez kindly reviewed an earlier version of this manuscript. We are very grateful to suggestions and helpful discussions by Prof. Mohsen Eliasi and Prof. Reza Nozaeim on tectonic topics in this paper. Dear Prof. Leon E Long is so appreciated for proofreading and editing the revised manuscript. We would like to thank Prof. Chad Deering for editorial handling of the paper and two anonymous reviewers for their in-depth reviews and constructive comments.

References

Agard P, Omrani J, Jolivet L and Mouthereau F (2005) Convergence history across Zagros (Iran): constraints from collisional and earlier deformation. *International Journal of Earth Sciences* **94**, 401–19.

Agard P, Omrani J, Jolivet L, Whitechurc H, Vrielynck B, Spakman W, Monié P, Meyer B and Wortel R (2011) Zagros orogeny: a subduction-dominated process. *Geological Magazine* **148**, 692–725.

Aghanabati A (2004) *Geology of Iran*. Tehran: Geological Survey of Iran Publication.

Alavi M (1994) Tectonics of the Zagros orogenic belt of Iran: new data and interpretations. *Tectonophysics* **229**, 211–38.

Alavi M (2004) Regional stratigraphy of the Zagros fold-thrust belt of Iran and its proforeland evolution. *American Journal of Science* **304**, 1–20.

Alavi M (2007) Structures of the Zagros fold-thrust belt in Iran. *American Journal of Science* **307**, 1064–95.

Aranguren A (1997) Magnetic fabric and 3D geometry of the Hombreiro-Sta. Eulaliapluton: implications for the Variscan structures of eastern Galicia, NW Spain. *Tectonophysics* **273**, 329–44.

Archanjo BS, Barboza APM, Neves BRA, Malard LM, Ferreira EHM, Brant JC, Alves ES, Plentz F, Carozo V, Fragneaud B, Maciel IO, Almeida CM, Jorio A and Achete CA (2012) The use of a Ga+ focused ion beam to modify graphene for device applications. *Nanotechnology* **23**, 255305, doi: 10.1088/0957-4484/23/25/255305.

Archanjo CJ and Launeau P (2004) Magma flow inferred from preferred orientations of plagioclase of the Rio Ceará-Mirim dyke swarm (NE Brazil) and its AMS significance. In *Magnetic Fabric: Methods and*

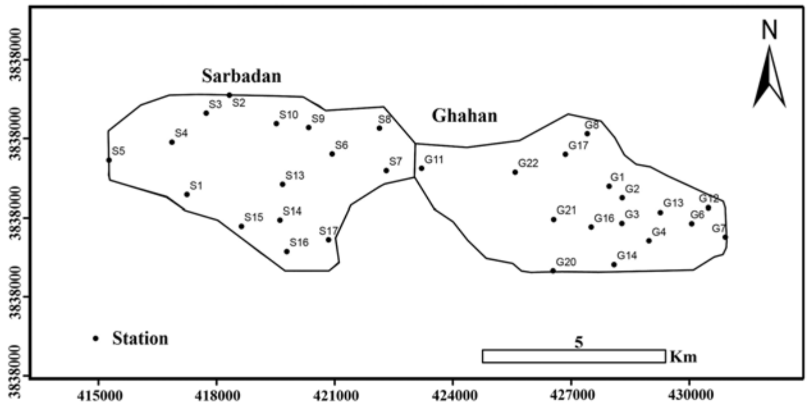

Fig. 10. Location of sampling stations used for the magnetic fabric study in the Sarbadan (S) and Ghahan (G) stocks.

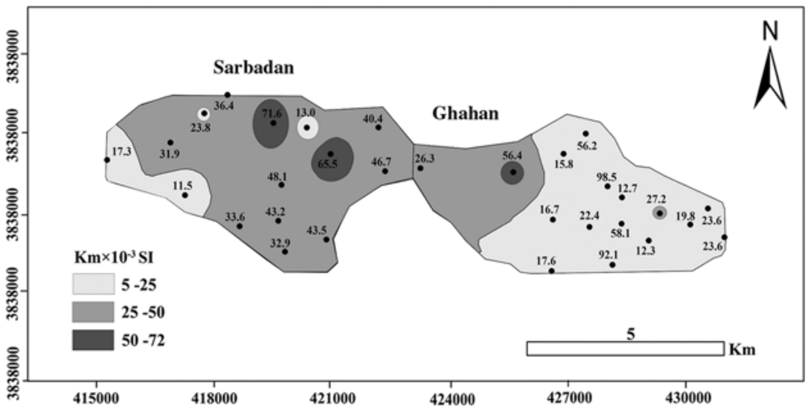

Fig. 11. Contour map of magnetic susceptibility (Km) for the Ghahan and Sarbadan stocks.

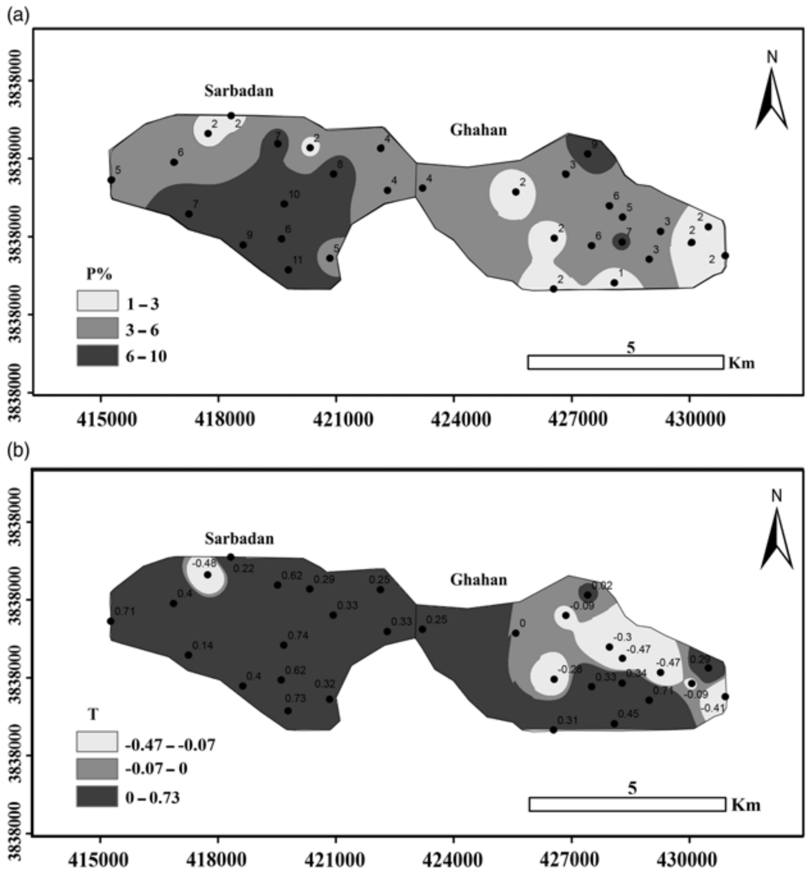

Fig. 12. (a) Contour maps of anisotropy percentage (P%) and (b) shape parameter (T) for the Ghahan and Sarbadan stocks.

https://doi.org/10.1017/S0016756818000766 Published online by Cambridge University Press

Table 4. A summary of the AMS results on intrusive rocks in Iran

Pluton	Age (Ma)	Long/Lat	Structural zone	Composition	Type	Km (× 10−3 SI)	P%	T	Model of emplacement	References
Zahedan	32	60.71 29.33	Southeast Iran	Diorite to granite	I-type	0.075–8.1 (mean 2.3)	0.3–38.4 (mean 9.5)	Oblate	Syntectonic sill in a transtensional setting	Sadeghian *et al.* (2005)
Shah-Kuh	176	59.22 31.72	Central Iran	Granodiorite and syenogranite	S-type	0.034–0.317 (mean 0.166)	0.3–8.6 (mean 2.78)	Oblate	Shear zone	Esmaeily *et al.* (2007)
Urumieh	80	45.15 37.15	SSZ	Diorite and biotite-granite	I-type	0.022–34 (mean 3.4)	0.15–26 mean 3.75	Oblate	Dextral transpressive	Ghalamghash *et al.* (2009)
Shir-Kuh	136	54.01 31.67	Central Iran	Granodiorite to leucogranite	S-type	0.02–0.332 (mean 0.193)	0.4–5.7 (mean 1.79)	Oblate	Dextral shear along back-arc environment above the subducting Neo-Tethys	Sheibi *et al.* (2012)
Boroujerd and Gousheh	175 and 35	48.78 33.94	SSZ	Monzogranite, granodiorite, and quartz diorite	S-type	0.014–0.922 (mean 0.212)	0.4–12.1 (mean 3.74)	Homogeneous	Transpressive syntectonic regime during oblique subduction of the western Neo-Tethys under central Iran	Rasouli *et al.* (2012)
Tafresh	20	50.17 34.73	UDMA	Diorite-granodiorite	I-type	56.2–71.6 (mean 27.9)	1.2–11.4 (mean 4.87)	Oblate	Shear zone	This study

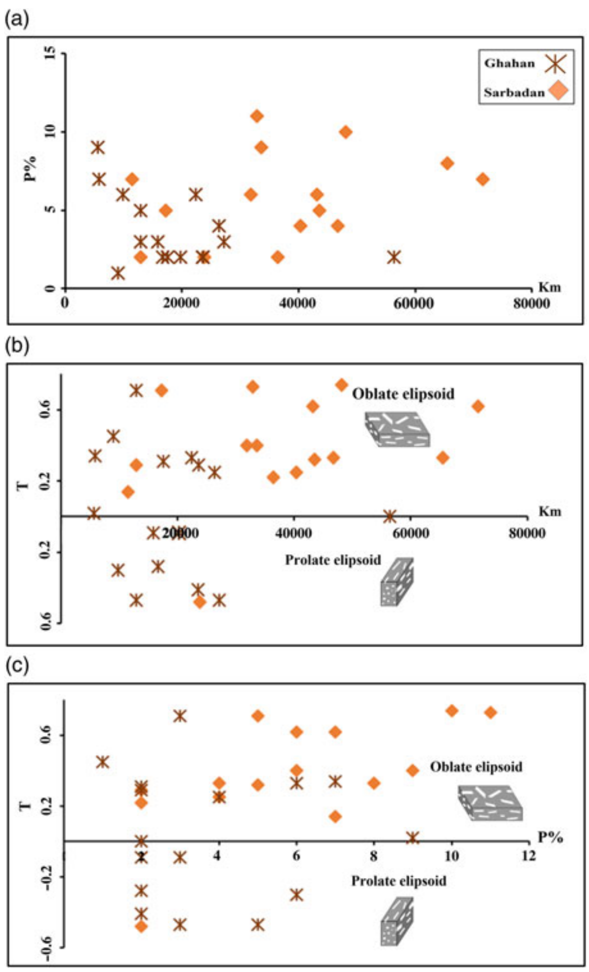

Fig. 13. (Colour online) Magnetic parameter diagrams. (a) P% v. Km; (b) T v. Km; (c) T v. P%.

Applications (eds F Martín-Hernández, CM Lüneberg, C Aubourg and M Jackson), pp. 285–98. Geological Society of London, Special Publication no. 238.

Beck Jr. ME (1983) On the mechanism of tectonic transport in zones of oblique subduction. *Tectonophysics* **93**, 1–11.

Bella Nké BE, Njanko T, Kwékam M, Njonfang E, Naba S, Tcheumenak KJ, Gountié M, Rochette P and Nédélec A (2014) Structural study of the Foréké-Dschang trachytic dome (Mount Bambouto, West Cameroon): an anisotropy of magnetic susceptibility (AMS) approach. *Journal of African Earth Sciences* **95**, 63–76.

Berberian M (1995) Master "blind" thrust faults hidden under the Zagros folds: active basement tectonics and surface morphotectonics. *Tectonophysics* **241**, 193–224.

Berberian F and Berberian M (1981) Tectono-plutonic episodes in Iran. In *Zagros, Hindu Kush, Himalaya: Geodynamic Evolution* (eds HK Gupta and FM Delaney), pp. 5–32. Washington, DC: American Geophysical Union.

Berberian M and King GCP (1981) Towards a paleogeography and tectonic evolution of Iran. *Canadian Journal of Earth Sciences* **18**, 210–65.

Berberian F, Muir ID, Pankhurst RJ and Berberian M (1982) Late Cretaceous and early Miocene Andean-type plutonic activity in northern Makran and Central Iran. *Journal of the Geological Society, London* **139**, 605–14.

Borg LE, Clynne MA and Bullen TD (1997) The variable role of slab-derived fluids in the generation of a suite of primitive calc-alkaline lavas from the southernmost Cascades, California. *The Canadian Mineralogist* **35**, 425–52.

Borradaile GJ (1988) Magnetic susceptibility, petrofabrics and strain. *Tectonophysics* **156**, 1–20.

Bouchez JL (1997) Granite is never isotropic: an introduction to AMS studies of granitic rocks. In *Granite: From Segregation of Melt to Emplacement Fabrics* (eds J-L Bouchez, D Hutton and WE Stephens), pp. 95–112. Netherlands: Springer.

Bouchez JL (2000) Anisotropie de susceptibilité magnétique et fabrique des granites. *Comptes Rendus de l'Académie des Sciences, Series IIA – Earth and Planetary Science* **330**, 1–14.

Bouchez JL, Gleizes G, Djouadi T and Rochette P (1990) Microstructure and magnetic susceptibility applied to emplacement kinematics of granites: the example of the Foix pluton (French Pyrenees). *Tectonophysics* **184**, 157–71.

Brown M and Solar GS (1998) Granite ascent and emplacement during contractional deformation in convergent orogens. *Journal of Structural Geology* **20**, 1365–93.

https://doi.org/10.1017/S0016756818000766 Published online by Cambridge University Press

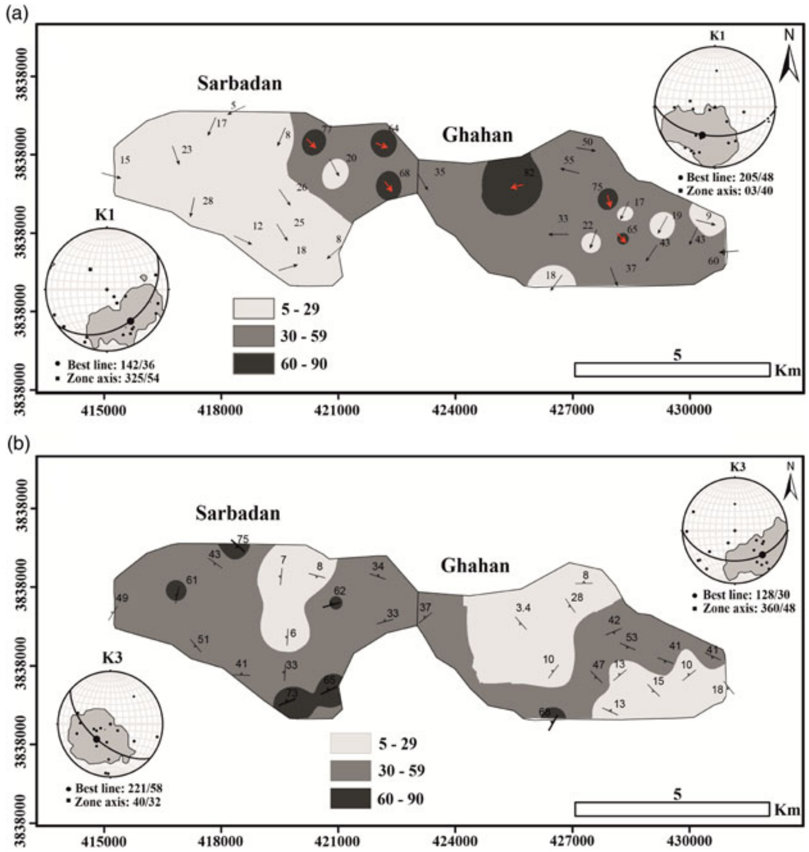

Fig. 14. (Colour online) (a) Magnetic lineation and (b) foliation maps of the Sarbadan and Ghahan stocks. Stereoplots represent the lineations (K1) and pole to foliation planes (K3).

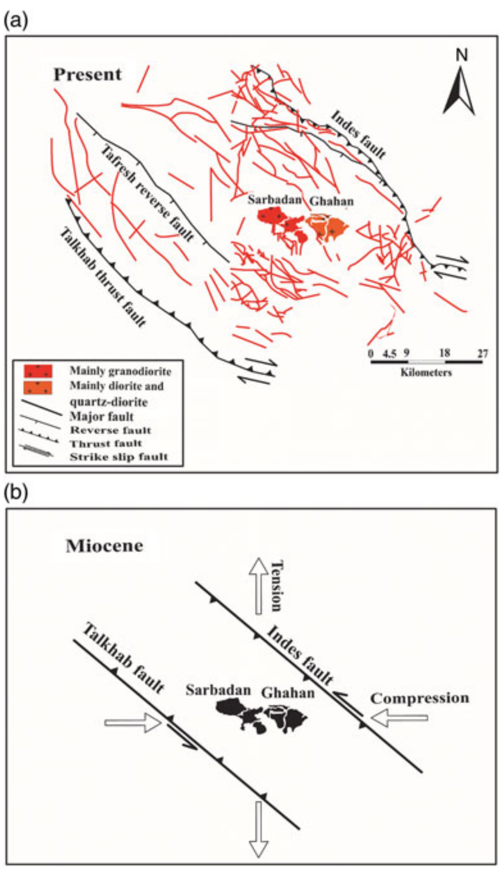

Fig. 15. (Colour online) (a) Location and movement of the Indes and Talkhab faults in the Tafresh area, and (b) the idealized model for emplacement of the Tafresh granitoids.

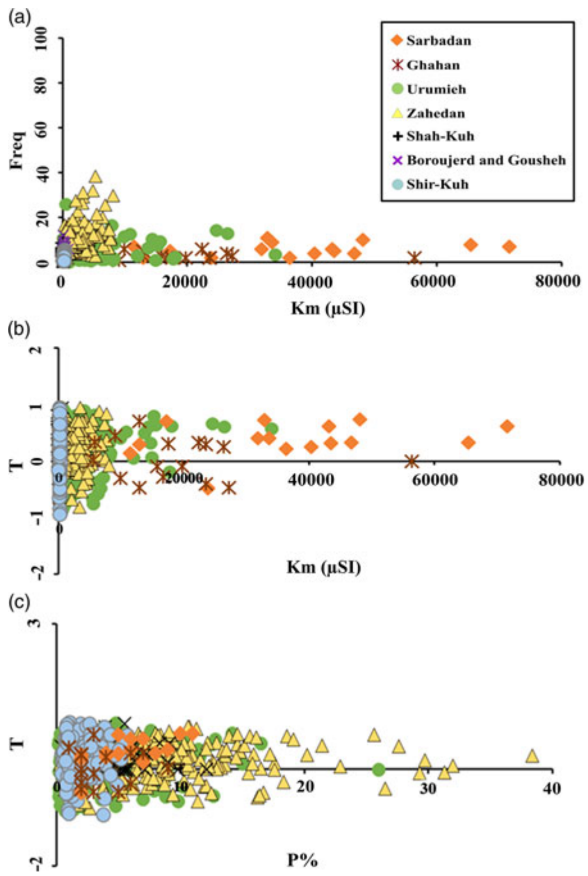

Fig. 16. (Colour online) Magnetic parameter diagrams. (a) Frequency v. Km; (b) T v. Km; (c) T v. P%.

https://doi.org/10.1017/S0016756818000766 Published online by Cambridge University Press

Buddington AF and Lindsley DH (1964) Iron-titanium oxide minerals and synthetic equivalents. *Journal of Petrology* **5**, 310–57.

Cañón-Tapia E and Chávez-Álvarez MJ (2004) Rotation of uniaxial ellipsoidal particles during simple shear revisited: the influence of elongation ratio, initial distribution of a multiparticle system and amount of shear in the acquisition of a stable orientation. *Journal of Structural Geology* **26**, 2073–87.

Cañón-Tapia E and Coe R (2002) Rock magnetic evidence of inflation of a flood basalt lava flow. *Bulletin of Volcanology* **64**, 289–302.

Cañón-Tapia E, Walker GP and Herrero-Bervera E (1996) The internal structure of lava flows—insights from AMS measurements I: near-vent a'a. *Journal of Volcanology and Geothermal Research* **70**, 21–36.

Cañón-Tapia E, Walker GP and Herrero-Bervera E (1997) The internal structure of lava flows insights from AMS measurements II: Hawaiian pahoehoe, toothpaste lava and 'a'ā. *Journal of Volcanology and Geothermal Research* **76**, 19–46.

Chappell BW and White AJR (2001) Two contrasting granite types: 25 years later. *Australian Journal of Earth Sciences* **48**, 489–99.

Corti G, Moratti G and Sani F (2005) Relations between surface faulting and granite intrusions in analogue models of strike-slip deformation. *Journal of Structural Geology* **27**, 1547–62.

Cruden AR and Launeau P (1994) Structure, magnetic fabric and emplacement of the Archean Lebel Stock, SW Abitibi greenstone belt. *Journal of Structural Geology* **16**, 677–91.

Cruden AR, Tobisch OT and Launeau P (1999) Magnetic fabric evidence for conduit-fed emplacement of a tabular intrusion: Dinkey Creek Pluton, central Sierra Nevada batholith, California. *Journal of Geophysical Research: Solid Earth* **104**, 10511–30.

Dercourt JEA, Zonenshain LP, Ricou L, Kazmin VG, Le Pichon X, Knipper AL, Grandjacquet C, Sbortshikov IM, Geyssant J, Lepvrier C and Pechersky DH (1986) Geological evolution of the Tethys belt from the Atlantic to the Pamirs since the Lias. *Tectonophysics* **123**, 241–315.

De Saint-Blanquat M, Habert G, Horsman E, Morgan SS, Tikoff B, Launeau P and Gleizes G (2006) Mechanisms and duration of non-tectonically assisted magma emplacement in the upper crust: the Black Mesa pluton, Henry Mountains, Utah. *Tectonophysics* **428**, 1–31.

De Saint-Blanquat M, Law RD, Bouchez JL and Morgan SS (2001) Internal structure and emplacement of the Papoose Flat pluton: an integrated structural, petrographic, and magnetic susceptibility study. *Geological Society of America Bulletin* **113**, 976–95.

De Saint-Blanquat M, Tikoff B, Teyssier C and Vigneresse JL (1998) Transpressional kinematics and magmatic arcs. In *Continental Transpressional and Transtensional Tectonics* (eds RE Holdsworth, RA Strachan and JF Dewey), pp. 327–40. Geological Society, London, Special Publication no. 135.

Dragoni M, Lanza R and Tallarico A (1997) Magnetic anisotropy produced by magma flow: theoretical model and experimental data from Ferrar dolerite sills (Antarctica). *Geophysical Journal International* **128**, 230–40.

Ellwood BB (1978) Flow and emplacement direction determined for selected basaltic bodies using magnetic susceptibility anisotropy measurements. *Earth and Planetary Science Letters* **41**, 254–64.

Ellwood BB, Whitney JA, Wenner DB, Mose D and Amerigian C (1980) Age, paleomagnetism, and tectonic significance of the Elberton Granite, Northeast Georgia Piedmont. *Journal of Geophysical Research: Solid Earth* **85**, 6521–33.

Eriksson PI, Riishuus MS, Sigmundsson F, and Elming SA (2011) Magma flow directions inferred from field evidence and magnetic fabric studies of the Streitishvarf composite dike in east Iceland. *Journal of Volcanology and Geothermal Research* **206**, 30–45.

Esmaeily D, Bouchez JL and Siqueira R (2007) Magnetic fabrics and microstructures of the Jurassic Shah-Kuh granite pluton (Lut Block, Eastern Iran) and geodynamic inference. *Tectonophysics* **439**, 149–70.

Förster H, Fesefeldt K and Kürsten M (1972) Magmatic and orogenic evolution of the central Iranian volcanic belt. In *Proceedings of the 24th International Geology Congress, Section 2*, pp. 198–210. Montreal: The Congress.

Ghalamghash J, Nédélec A, Bellon H, Vousoughi Abedini M and Bouchez JL (2009) The Urumieh plutonic complex (NW Iran): a record of the geodynamic evolution of the Sanandaj–Sirjan zone during Cretaceous times–Part I: petrogenesis and K/Ar dating. *Journal of Asian Earth Sciences* **35**, 401–15.

Glazner AF, Bartley JM, Coleman DS, Gray W and Taylor RZ (2004) Are plutons assembled over millions of years by amalgamation from small magma chambers? *GSA Today* **14**, 4–12.

Gleizes G, Nédélec A, Bouchez JL, Autran A and Rochette P (1993) Magnetic susceptibility of the Mont-Louis Andorra ilmenite-type granite (Pyrenees): a new tool for the petrographic characterization and regional mapping of zoned granite plutons. *Journal of Geophysical Research: Solid Earth* **98**, 4317–31.

Golonka J (2004) Plate tectonic evolution of the southern margin of Eurasia in the Mesozoic and Cenozoic. *Tectonophysics* **381**, 235–73.

Guillet P, Bouchez JL and Wagner JJ (1983) Anisotropy of magnetic susceptibility and magmatic structures in the Guerande granite massif (France). *Tectonics* **2**, 419–29.

Guineberteau B, Bouchez JL and Vigneresse JL (1987) The Mortagne granite pluton (France) emplaced by pull-apart along a shear zone: structural and gravimetric arguments and regional implication. *Geological Society of America Bulletin* **99**, 763–70.

Hajian H (1977) *Geological Map of the Tafresh Area, Scale 1:100000*. Iran: Geological Survey of Iran.

Hanson GN (1980) Rare earth elements in petrogenetic studies of igneous systems. *Annual Review of Earth and Planetary Sciences* **8**, 371–406.

Hutton DH (1988) Granite emplacement mechanisms and tectonic controls: inferences from deformation studies. *Earth and Environmental Science Transactions of the Royal Society of Edinburgh* **79**, 245–55.

Irvine TN and Baragar WRA (1971) A guide to the chemical classification of the common volcanic rocks. *Canadian Journal of Earth Sciences* **8**, 523–48.

Ishihara S (1977) The magnetite-series and ilmenite-series granitic rocks. *Mining Geology* **27**, 293–305.

Jarrard RD (1986) Terrane motion by strike-slip faulting of forearc slivers. *Geology* **14**, 780–3.

Jelínek V (1981) Characterization of the magnetic fabric of rocks. *Tectonophysics* **79**, 63–7.

Jelínek V and Kropáček RV (1978) Statistical processing of anisotropy of magnetic susceptibility measured on groups of specimens. *Studia Geophysica et Geodaetica* **22**, 50–62.

Kamenetsky VS, Everard JL, Crawford AJ, Varne R, Eggins SM and Lanyon R (2000) Enriched end-member of primitive MORB melts: petrology and geochemistry of glasses from Macquarie Island (SW Pacific). *Journal of Petrology* **41**, 411–30.

Khan MA (1962) The anisotropy of magnetic susceptibility of some igneous and metamorphic rocks. *Journal of Geophysical Research* **67**, 2873–85.

Lallemand S and Jolivet L (1986) Japan Sea: a pull-apart basin? *Earth and Planetary Science Letters* **76**, 375–89.

Langmuir CH, Bender JF, Bence AE, Hanson GN and Taylor SR (1977) Petrogenesis of basalts from the famous area: mid-Atlantic Ridge. *Earth and Planetary Science Letters* **36**, 133–56.

Lanza R and Meloni A (2006) *The Earth's Magnetic Field: An Introduction for Geologists*. Heidelberg: Springer.

Le Roex AP (1987) Source regions of mid-ocean ridge basalts: evidence for enrichment processes. In *Mantle Metasomatism* (eds MA Menzies and CJ Hawkesworth), pp. 398–422. London: Academic Press.

Masson F, Anvari M, Djamour Y, Walpersdorf A, Tavakoli F, Daignières M, Nankali H and Van Gorp S (2007) Large-scale velocity field and strain tensor in Iran inferred from GPS measurements: new insight for the present-day deformation pattern within NE Iran. *Geophysical Journal International* **170**, 436–40.

McDonough WF and Sun SS (1995) The composition of the Earth. *Chemical Geology* **120**, 223–53.

Mégard F (1987) Cordilleran Andes and Marginal Andes: a review of Andean geology north of the Arica Elbow (18) S. *Circum-Pacific Orogenic Belts and Evolution of the Pacific Ocean Basin* **18**, 71–95.

Middlemost EAK (1991) Towards a comprehensive classification of igneous rocks and magmas. *Earth-Science Reviews* **31**, 73–87.

Morley CK, Kongwung B, Julapour AA, Abdolghafourian M, Hajian M, Waples D, Warren J, Otterdoom H, Srisuriyon K and Kazemi H (2009) Structural development of a major late Cenozoic basin and transpressional belt in central Iran: the Central Basin in the Qom-Saveh area. *Geosphere* **5**, 325–62.

Owens WH (1974) Mathematical model studies on factors affecting the magnetic anisotropy of deformed rocks. *Tectonophysics* **24**, 115–31.

https://doi.org/10.1017/S0016756818000766 Published online by Cambridge University Press

Pearce JA (1983) Role of the sub-continental lithosphere in magma genesis at active continental margins. In *Continental Basalts and Mantle Xenoliths* (eds CJ Hawkesworth and MJ Norry), pp. 230–49. Nantwich, Cheshire: Shiva Publications.

Pearce JA, Harris NB and Tindle AG (1984) Trace element discrimination diagrams for the tectonic interpretation of granitic rocks. *Journal of Petrology* **25**, 956–83.

Rajabioun J (2000) *Brittle deformation analysis in Tafresh area with emphasize paleostress reconstruction*. M.Sc. thesis, Tarbiat Modares University, Iran, 92 pp. Published thesis (in Persian).

Rasouli J, Ahadnejad V and Esmaeily D (2012) A preliminary study of the anisotropy of magnetic susceptibility (AMS) of Boroujerd granitoids, Sanandaj-Sirjan Zone, West Iran. *Natural Science* **4**, 91–105.

Regard V, Bellier O, Thomas JC, Bourles D, Bonnet S, Abbassi MR, Braucher R, Mercier J, Shabanian E, Soleymani S and Feghhi K (2005) Cumulative right-lateral fault slip rate across the Zagros-Makran transfer zone: role of the Minab-Zendan fault system in accommodating Arabia—Eurasia convergence in southeast Iran. *Geophysical Journal International* **162**, 177–203.

Rezaei-Kahkhaei M, Galindo C, Pankhurst RJ and Esmaeily D (2011) Magmatic differentiation in the calc-alkaline Khalkhab–Neshveh pluton, Central Iran. *Journal of Asian Earth Sciences* **42**, 499–514.

Ricou LE, Braud J and Brunn J (1977) Le Zagros. In *Livre à la Mémoire de Albert F. de Lapparent*, pp. 33–52. Société géologique de France, Mémoire Hors-Séries Vol. 8.

Rochette P, Aubourg C and Perrin M (1999) Is this magnetic fabric normal? A review and case studies in volcanic formations. *Tectonophysics* **307**, 219–34.

Rochette P, Jackson M and Aubourg C (1992) Rock magnetism and the interpretation of anisotropy of magnetic susceptibility. *Reviews of Geophysics* **30**, 209–26.

Rogers G and Hawkesworth CJ (1989) A geochemical traverse across the North Chilean Andes: evidence for crust generation from the mantle wedge. *Earth and Planetary Science Letters* **91**, 271–85.

Sadeghian M, Bouchez JL, Nédélec A, Siqueira R and Valizadeh MV (2005) The granite pluton of Zahedan (SE Iran): a petrological and magnetic fabric study of a syntectonic sill emplaced in a transtensional setting. *Journal of Asian Earth Sciences* **25**, 301–27.

Sadeghian M, Sheibi M and Badallo S (2014) The emplacement mechanism of the Gol-e-Zard granodiorite pluton, north of Aligoudarz, west of Iran, by using of AMS method. *Scientific Quarterly Journal, Geosciences* **23**, 129–42 (in Persian).

Sajona FG, Maury RC, Bellon H, Cotten J and Defant M (1996) High field strength element enrichment of Pliocene–Pleistocene island arc basalts, Zamboanga Peninsula, Western Mindanao (Philippines). *Journal of Petrology* **37**, 693–726.

Schöpa A, Floess D, De Saint-Blanquat M, Annen C and Launeau P (2015) The relation between magnetite and silicate fabric in granitoids of the Adamello Batholith. *Tectonophysics* **642**, 1–15.

Shafaii Moghadam HS and Stern RJ (2011) Geodynamic evolution of Upper Cretaceous Zagros ophiolites: formation of oceanic lithosphere above a nascent subduction zone. *Geological Magazine* **148**, 762–801.

Shand SJ (1943) *Eruptive Rocks: Their Genesis, Composition, and Classification, with a Chapter on Meteorites*. New York: Hafner Publishing.

Sheibi M, Bouchez JL, Esmaeily D and Siqueira R (2012) The Shir-Kuh pluton (Central Iran): magnetic fabric evidences for the coalescence of magma batches during emplacement. *Journal of Asian Earth Sciences* **46**, 39–51.

Sheibi M and Majidi P (2015) Emplacement mechanism of the Challu granitoids pluton using magnetite fabric method, southern Damghan. *Scientific Quarterly Journal, Geosciences* **24**, 87–98 (in Persian).

Sheibi M and Pooralizadeh Moghadam M (2015) Emplacement mechanism of the Panj-Kuh granitoid pluton using magnetic fabric method. *Scientific Quarterly Journal, Geosciences* **24**, 117–27 (in Persian).

Stacey FD (1962) Theory of the magnetic susceptibility of stressed rock. *Philosophical Magazine* **7**, 551–6.

Stöcklin J (1968) Structural history and tectonics of Iran: a review. *American Association of Petroleum Geologists Bulletin* **52**, 1229–58.

Sun SS and McDonough WS (1989) Chemical and isotopic systematics of oceanic basalts: implications for mantle composition and processes. In *Magmatism in the Ocean Basins* (eds AD Saunders and MJ Norry), pp. 313–45. Geological Society of London, Special Publication no. 42.

Tarling DH and Hrouda F (1993) *The Magnetic Anisotropy of Rocks*. London: Springer Science & Business Media.

Tcheumenak Kouémo J, Njanko T, Kwékam M, Naba S, Bella Nké BE, Yakeu Sandjo AF, Fozing EM and Njonfang E (2014) Kinematic evolution of the Fodjomekwet-Fotouni Shear Zone (West-Cameroon): implications for emplacement of the Fomopéa and Bandja plutons. *Journal of African Earth Sciences* **99**, 261–75.

Uyeda S, Fuller MD, Belshe JC and Girdler RW (1963) Anisotropy of magnetic susceptibility of rocks and minerals. *Journal of Geophysical Research* **68**, 279–91.

Whalen JB, Currie KL and Chappell BW (1987) A-type granites: geochemical characteristics, discrimination and petrogenesis. *Contributions to Mineralogy and Petrology* **95**, 407–19.

Whitney DL and Evans BW (2010) Abbreviations for names of rock-forming minerals. *American Mineralogist* **95**, 185–7.

Yakeu Sandjo AF, Njanko T, Njonfang E, Errami E, Rochette P and Fozing E (2016) Transpressional granite-emplacement model: structural and magnetic study of the Pan-African Bandja granitic pluton (West Cameroon). *Journal of Earth System Science* **125**, 179–202.